

Characterization of Palladium Nanoparticles by Using X-ray Reflectivity, EXAFS, and Electron Microscopy

Yuan Sun,[†] Anatoly I. Frenkel,[‡] Rebecca Isseroff,[§] Cheryl Shonbrun,^{‡,§} Michelle Forman,[§] Kwanwoo Shin,^{||} Tadanori Koga,[†] Henry White,[†] Lihua Zhang,[⊥] Yimei Zhu,[⊥] Miriam H. Rafailovich,^{*,†} and Jonathan C. Sokolov[†]

Department of Materials Science and Engineering, State University of New York at Stony Brook, Stony Brook, New York 11794-2275, Department of Physics, Yeshiva University, New York, New York 10016, Stella K. Abraham High School, Hewlett, New York 11557, Department of Materials Science and Engineering, K-JIST, Oryong-dong, Buk-gu, Kwang-ju, 500-712, Korea, and Brookhaven National Laboratory, Upton, New York 11973

Received October 4, 2005

We compared the characteristics of dodecanethiolate palladium nanoparticles synthesized by two different techniques, a one-phase method and a two-phase method. From transmission electron microscopy (TEM), we determined that the particle sizes were 46 ± 10 Å and 20 ± 5 Å for the one- and two-phase particles, respectively. Electron diffraction confirmed that their structure was face-centered cubic (fcc). The lattice constant a_0 was 3.98 ± 0.01 Å and 3.90 ± 0.01 Å for the one- and two-phase particles, respectively. High-resolution TEM (HRTEM) showed that the one-phase particles had an ordered core surrounded by a disordered shell structure, while the two-phase particles appeared to be crystalline throughout. The particles were also analyzed with extended X-ray absorption fine structure (EXAFS). A cuboctahedral fcc model was used to fit the data, which implied particle sizes of less than 10 Å for both the one- and two-phase particles. The discrepancy between the two techniques was attributed to the presence of a disordered phase, which we presumed was composed of Pd–S compounds. Compared with the bulk palladium, lattice expansion was observed in both one- and two-phase particles by electron diffraction, HRTEM, and EXAFS. At the air/water interface, a uniform film that produced surface pressure/area isotherms could only be obtained from the two-phase particles. The one-phase particles did not wet the water surface. X-ray reflectivity data indicated that the Langmuir monolayer of the two-phase particles was only 13 Å thick. TEM revealed the diameter of the particles in this layer to be 23 Å; hence the particles assumed an oblate structure after spreading. EXAFS examination of a stack of 750 Langmuir monolayers indicated far fewer Pd–S compounds, which may have dissolved in the water. The data were consistent with a model of a monolayer of truncated cuboctahedron Pd particles that were 7 Å thick and 19 Å in diameter.

Introduction

Palladium nanoparticles have received considerable attention due to their potential applications in catalysts,^{1,2} magnetic storage materials,³ and hydrogen storage materials.⁴

A variety of techniques have been utilized to prepare palladium nanoparticles, such as photolytic decomposition,⁵ thermal decomposition,⁶ sonochemical reduction,⁷ hydrogen reduction,⁸ electrochemical deposition,⁹ and so on. Since Brust et al.¹⁰ developed a two-phase method, monolayer-protected nanoclusters

(MPCs) have gained significant attention due to their high stability compared with conventional colloidal particles. More recently, Yee et al.¹¹ reported a one-phase synthetic procedure to generate gold and palladium nanoparticles stabilized by a mercaptoorganic monolayer, which are very similar to the MPCs made from the two-phase method. Previous research on gold MPCs reveals that the sulfur atoms bond with surface gold atoms via chemisorption, and the thiolate monolayers are three-dimensional (3D) analogues of the self-assembled monolayers (SAMs) on the two-dimensional (2D) gold surfaces.^{12,13} The particle size of gold MPCs can be controlled by the experimental parameters, especially the molar ratio of thiol to gold precursor.¹⁴ As for the synthesis of palladium MPCs, Murray et al.¹⁵ reported that, when the thiol/Pd ratio is 1:1 or lower, the product behaved quite similarly to Au MPCs; However, when synthesized with thiol/Pd ratio of 2:1 or higher,

* Corresponding author. E-mail: mrafailovich@notes.cc.sunysb.edu.

[†] State University of New York at Stony Brook.

[‡] Yeshiva University.

[§] Stella K. Abraham High School.

^{||} K-JIST.

[⊥] Brookhaven National Laboratory.

(1) Starà, I.; Nehasil, V.; Matolín, V. *Surf. Sci.* **1995**, *333*, 173–177.

(2) Valden, M.; Aaltonen, J.; Kuusisto, E.; Pessa, M.; Barnes, C. J. *Surf. Sci.* **1994**, *307*, 193–198.

(3) Taniyama, T.; Ohta, E.; Sato, T. *Europhys. Lett.* **1997**, *38*, 195–200.

(4) (a) Király, Z.; Mastalir, A.; Berger, F.; Dékány, I. *Langmuir* **1997**, *13*, 465–468. (b) Király, Z.; Mastalir, A.; Berger, F.; Dékány, I. *Langmuir* **1998**, *14*, 1281–1282.

(5) Narayan, A.; Landstrom, L.; Boman, M. *Appl. Surf. Sci.* **2003**, *208*, 137–141.

(6) Kim, S.-W.; Park, J.; Jang, Y.; Chung, Y.; Hwang, S.; Hyeon, T.; Kim, Y. W. *Nano Lett.* **2003**, *3*, 1289–1291.

(7) Dhas, N. A.; Gedanken, A. *J. Mater. Chem.* **1998**, *8*, 445.

(8) Schmid, G.; Harms, M.; Malm, J.-O.; Bovin, J.-O.; van Ruitenbeck, J.; Zandbergen, H. W.; Fu, W. T. *J. Am. Chem. Soc.* **1993**, *115*, 2046.

(9) Reetz, M. T.; Helbig, W. *J. Am. Chem. Soc.* **1994**, *116*, 7401.

(10) Brust, M.; Walker, M.; Bethell, D.; Schiffrin, D. J.; Whyman, R. *J. Chem. Soc., Chem. Commun.* **1994**, 801–802.

(11) Yee, C. K.; Jordan, R.; Ulman, A.; White, H.; King, A.; Rafailovich, M.; Sokolov, J. *Langmuir* **1999**, *15*, 3486–3491.

(12) (a) Dubois, L. H.; Nuzzo, R. G. *Annu. Rev. Phys. Chem.* **1992**, *43*, 437–463. (b) Poirier, G. E. *Chem. Rev.* **1997**, *97*, 1117–1127.

(13) (a) Terrill, R. H.; Postlethwaite, T. A.; Chen, C.-H.; Poon, C.-D.; Terzis, A.; Chen, A.; Hutchison, J. E.; Clark, M. R.; Wignall, G.; Londono, J. D.; Superfine, R.; Falvo, M.; Johnson, C. S., Jr.; Samulski, E. T.; Murray, R. W. *J. Am. Chem. Soc.* **1995**, *117*, 12537–12548. (b) Hostetler, M. J.; Stokes, J. J.; Murray, R. W. *Langmuir* **1996**, *12*, 3604–3612.

(14) (a) Leff, D. V.; Ohara, P. C.; Heath, J. R.; Gelbart, W. M. *J. Phys. Chem.* **1995**, *99*, 7036–7041. (b) Hostetler, M. J.; Wingate, J. E.; Zhong, C.-J.; Harris, J. E.; Vachet, R. W.; Clark, M. R.; Londono, J. D.; Green, S. J.; Stokes, J. J.; Wignall, G. D.; Glish, G. L.; Porter, M. D.; Evans, N. D.; Murray, R. W. *Langmuir* **1998**, *14*, 17–30.

(15) Zamborini, F. P.; Gross, S. M.; Murray, R. W. *Langmuir* **2001**, *17*, 481–488.

the product is either some form of Pd(II) alkanethiolate complex or extremely small Pd(0) clusters. On the other hand, a compound palladium–sulfide interphase is found to be present at the surface between the alkanethiolate SAM and the 2D palladium surface.¹⁶ This palladium–sulfide interphase enhances the SAM stability against the wet-chemical etchants compared with the alkanethiolate SAMs on Au.¹⁷ A recent study of Pd MPCs suggested that the surface of the Pd core is sulfurized to form a mixed Pd–S layer underneath the octadecanethiolate monolayer.¹⁸

Consequently, to understand the electronic and chemical properties of Pd nanoparticles, a systematic comparison between the results obtained by different synthetic techniques is needed. Here, we present a comparison between nanoparticles obtained via two synthetic techniques: a one-phase method developed by Yee et al.¹¹ and the more standard two-phase method developed by Brust et al.¹⁰ The particles are analyzed via a set of complementary methods: transmission electron microscopy (TEM) and electron diffraction are used to characterize the sizes and crystal structures, X-ray reflectivity (XR) and grazing incidence X-ray diffraction (GIXD) are used to study the thin film self-assembly at the air/water interface and/or as a Langmuir monolayer on solid substrates, and extended X-ray absorption fine structure (EXAFS) is used to study the radial distribution of the nearest neighbors.

Experimental Section

Particle Synthesis. The dodecanethiolate palladium nanoparticles (Pd–C12) were synthesized by using two methods: (1) a one-phase method developed by Yee et al. and (2) a two-phase method developed by Brust et al. Typically, in the one-phase method, 214 μL (0.891 mmol) of dodecanethiol was added under vigorous stirring (about 1000 rpm) to a solution of 200 mg (0.891 mmol) of palladium(II) acetate ($\text{Pd}(\text{C}_2\text{H}_3\text{O}_2)_2$) in 10 mL of freshly distilled, anhydrous THF. The mixture was stirred for about 30 min at room temperature. A solution of 10 mL 1.0 M of lithium triethylborohydride in THF was added at a rate of 0.1 mL/min. The mixture turned to dark brown. After being stirred for 3 h, the mixture was mixed with 40 mL of absolute ethanol to precipitate the nanoparticles. The particles were centrifuged and washed with ethanol four times and dried in a vacuum desiccator.

In the two-phase method, an aqueous solution of potassium palladium(II) chloride (K_2PdCl_4) (0.5 mmol in 20 mL of H_2O) was mixed with a solution of tetraoctylammonium bromide in toluene (2.4 mmol in 20 mL of toluene). The two-phase mixture was vigorously stirred until all the PdCl_4^{2-} was transferred into the organic layer. Dodecanethiol (120 μL , 0.5 mmol) was then added. A freshly prepared aqueous solution of sodium borohydride (6 mmol in 10 mL of water) was added at a rate of 2 mL/min under vigorous stirring (about 1000 rpm), the organic phase changed color from burnt orange to dark brown within a few minutes. After being stirred for 3 h, the organic phase was separated, evaporated to 5 mL in a rotary evaporator, and mixed with 160 mL of ethanol to remove excess thiol. The mixture was centrifuged to get the black precipitate, which was washed with ethanol four times and dried in a vacuum desiccator.

The octadecanethiolate palladium nanoparticles (Pd–C18) were synthesized by using the two-phase method only. All of the alkanethiolate palladium nanoparticles were used as-made with no further attempts to narrow the size distribution.

Measurement of Surface Pressure/Area Isotherm. Surface pressure/area isotherms were measured at room temperature by using a KSV 5000LB trough with a pair of automatically movable barriers. The water was purified by a Millipore Milli-Q system. A 200 μL

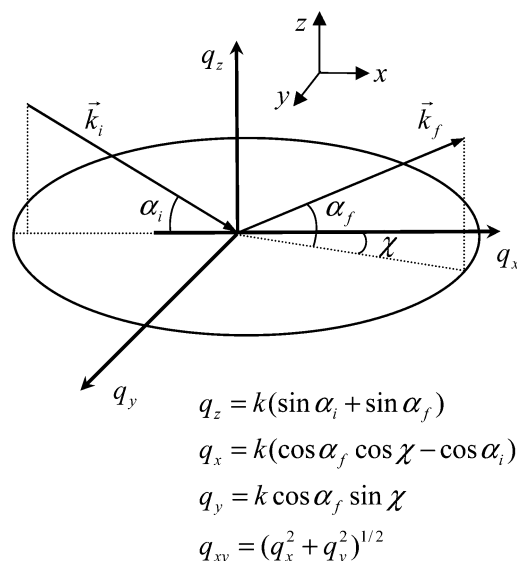


Figure 1. Scattering geometry of the wave vector components used in X-ray reflectivity and grazing incidence X-ray diffraction measurements.

solution of 1 mg/mL of nanoparticles in toluene was spread uniformly onto the air/water interface. After the toluene evaporated, the isotherm measurements were initiated by double-barrier compression at a rate of 5 mm/min.

TEM and HRTEM Characterization. TEM analysis was performed on a Philips CM12 TEM operating at 100 keV. HRTEM analysis was achieved on a JEOL 3000F operating at 300 keV, located at the Center for Functional Nanomaterials (CFN), Brookhaven National Laboratory. The samples were prepared in two different ways. A droplet of dilute solution of nanoparticles in toluene was evaporated onto the carbon-coated side of a 400-mesh copper TEM grid. For Langmuir films of nanoparticles, the edge of a grid was clamped with tweezers and brought parallel to the surface of the trough. The carbon-coated side was quickly contacted with the film surface and lifted off. Electron diffraction patterns were analyzed by POLAR (from STAR), a comprehensive software package for 2D X-ray/electron diffraction pattern analysis. HRTEM images were analyzed by WIMAGE developed by the TEM group in the CFN.

X-ray Reflectivity (XR) and Grazing Incidence X-ray Diffraction (GIXD). To study the Langmuir films of the nanoparticles formed under specific surface pressures, films were lifted from the water surface onto silicon wafers and measured by X-ray reflectivity and grazing incidence X-ray diffraction.

The scattering geometry of the wave vector components used in the experiments is shown in Figure 1. The z , x , y directions are defined as the normal to the sample surface and the in-plane and out-of plane directions perpendicular to the z axis, respectively. The wave-vector transfer, $\vec{q} = \vec{k}_f - \vec{k}_i$, with \vec{k}_f and \vec{k}_i the incident and scattered wave vectors, is controlled by varying the incident (α_i), exit (α_f), and in-plane detector (χ) angle. The components of \vec{q} are given by $q_z = k(\sin \alpha_i + \sin \alpha_f)$, $q_x = k(\cos \alpha_f \cos \chi - \cos \alpha_i)$, and $q_y = k \cos \alpha_f \sin \chi$, where k is defined by $k = 2\pi/\lambda$. The reciprocal lattice vector q_{xy} is given by $q_{xy} = \sqrt{q_x^2 + q_y^2}$. The absolute specular reflectivity is defined as the intensity taken at $q_x = 0$ as a function of q_z by varying α_i and α_f while maintaining $\alpha_i = \alpha_f$. Because the specular reflectivity detects the variation of the dispersion $\delta(z)$ in the direction of the surface normal, averaged in the (x,y) plane, it is sensitive to the layer thicknesses (t), the dispersion contrasts ($d\delta(z)/dz$), and the interfacial roughnesses (s). For GIXD measurements, the incident beam is fixed at an angle (α_i) about 80% of the critical angle. Compared to the specular reflectivity, which is sensitive to the dispersion profile $\delta(z)$ perpendicular to the interfaces, the GIXD measurement depends on the in-plane correlation of the two-dimensionally ordered palladium clusters. The lattice spacing can be derived from the diffraction peak position. By combining the

(16) Love, J. C.; Wolfe, D. B.; Haasch, R.; Chabinyk, M. L.; Paul, K. E.; Whitesides, G. M.; Nuzzo, R. G. *J. Am. Chem. Soc.* **2003**, *125*, 2597–2609.

(17) Love, J. C.; Wolfe, D. B.; Haasch, R.; Chabinyk, M. L.; Paul, K. E.; Whitesides, G. M. *J. Am. Chem. Soc.* **2002**, *124*, 1576–1577.

(18) Murayama, H.; Ichikuni, N.; Negishi, Y.; Nagata, T.; Tsukuda, T. *Chem. Phys. Lett.* **2003**, *376*, 26–32.

results from specular reflectivity and GIXD, the detailed out-of-plane and in-plane structure of palladium nanoparticles in the Langmuir films can be revealed.

The samples for X-ray measurements were prepared as follows. At the desired surface pressure, the Langmuir–Blodgett technique (a vertical lifting method) was used to transfer the Langmuir film of nanoparticles from the air/water interface onto a 2 in. \times 2 in. silicon wafer (treated by a sulfuric acid–hydrogen peroxide mixture), which was immersed in the pure water before the particle solution was spread, and then retracted at a speed of 2 mm/min. The specular reflectivity of the two-phase Pd–C12 Langmuir film was measured on beamline X10B of the National Synchrotron Light Source at Brookhaven National Laboratory, using a 0.2 mm \times 0.5 mm X-ray beam of wavelength $\lambda = 0.87$ Å. The XR and GIXD measurements of two-phase Pd–C18 Langmuir films were performed on the W1.1 reflectometer at the HASYLAB at the DESY in Germany, using an energy of 10.5 keV that corresponds to a wavelength of $\lambda = 1.18$ Å.

Extended X-ray Absorption Fine Structure (EXAFS). The X-ray absorption experiments were performed at the beamline X16C at the Brookhaven National Laboratory's National Synchrotron Light Source by using the Si(111) double-crystal monochromator.

X-ray absorption data from the Pd–C12 particles were collected in transmission mode at room temperature by scanning from 150 eV below to 1100 eV above the Pd K edge (24 350 eV). To prepare the sample, approximately 10 mg of the one-phase or two-phase Pd–C12 particles was spread uniformly on a piece of adhesive tape with a brush. The tape was folded several times to reach the appropriate thickness for transmission EXAFS experiment, corresponding to the Pd absorption K-edge step of ca. 1.0. The Ar-filled ionization chambers were used as the incident (15 cm long), transmission (30 cm long), and reference (30 cm long) X-ray detectors. The reference Pd foil was measured simultaneously in each scan in order to calibrate the X-ray energy for the scan alignment purpose. After energy alignment, approximately 10 scans were averaged and analyzed for each sample.

To obtain the Pd K-edge EXAFS spectra from the Langmuir films of two-phase Pd–C12 particles, we used fluorescence mode. To prepare the sample, 200 μ L of 1 mg/mL solution of two-phase Pd–C12 in toluene was spread onto the air/water interface. The Langmuir films were then lifted onto Kapton films at a surface pressure of 7.8 mN/m and at a speed of 2 mm/min. The Kapton films were then cut into small pieces and stacked to get approximately 750 layers of the Langmuir film in the EXAFS beam path. The five-grid, 8-cm-long, Ar-filled Lytle detector was used for fluorescence detection, and the same ionization chambers were used for the incident, transmission, and reference beam detectors, as in the transmission mode. After energy alignment, approximately 50 scans were averaged and analyzed.

The EXAFS data analysis was performed by IFEFFIT¹⁹ and described in detail below.

Results and Discussion

TEM, HRTEM, and Electron Diffraction. TEM images of the one- and two-phase Pd–C12 particles dried from dilute toluene solutions and deposited on TEM grids are shown in Figure 2. The particle diameter was measured by using UTHSCSA ImageTool and was plotted as a histogram. The one-phase Pd–C12 particles have a mean size of 46 ± 10 Å. The two-phase Pd–C12 particles have a smaller mean size of 20 ± 5 Å. It has been known that the molar ratio of palladium²⁰ or gold¹⁴ precursor to thiol is one of the most important factors that affect the size of the resulting nanoparticles. In our case, this ratio was fixed at 1:1 for both the one- and two-phase methods. Therefore, according to the TEM measurements, the size of the two-phase Pd–C12 particles was nearly one-half the size of one-phase

Pd–C12 particles based on the same Pd/thiol ratio. For the one-phase method, we also found that the particle size increased by 26% when the Pd/thiol ratio was increased to 3:1 (Figure 2c, f). However, the two-phase method, using a Pd/thiol ratio of 3:1, yielded a product that did not dissolve in toluene or polar solvents. Because we are not sure of the exact chemical nature of these particles, they will not be discussed further.

The electron diffraction pattern from the one-phase Pd–C12 particles is shown in Figure 2g. Although the diffraction intensities are weak and the rings blurred, this pattern can still be indexed unambiguously to an fcc structure with a cell parameter a_0 of 3.98 ± 0.01 Å. Figure 2h shows the electron diffraction pattern from the two-phase particles. This pattern shares the major features with the one from one-phase particles, except that the diffraction intensities are even weaker and fewer rings are observable. These differences are probably due to the smaller size of the two-phase particles, which can induce a greater degree of disorder. The diffraction pattern is indexed to an fcc structure with a cell parameter a_0 of 3.90 ± 0.01 Å. One can see that, for the one-phase particles, the cell parameter is larger than that of bulk palladium (3.8907 Å).²¹ This expansion is consistent with the results obtained from HRTEM and EXAFS that will be presented later.

The details of the internal structure of the particles were studied with HRTEM. As shown in Figure 3a, the HRTEM image of the one-phase particles reveals an ordered core surrounded by a relatively large disordered shell. Fast Fourier transform (FFT) was performed for the particle indicated by the arrow, giving d -spacing of 2.127 Å for (200) planes and 2.145 Å for (020) planes. These values suggest slight distortion of the ordered core. From the HRTEM images, we can obtain the average total diameter of the particles to be 45 ± 9 Å, which is in agreement with the value obtained from the low resolution images, and the diameter of the core to be only 26 ± 8 Å. Because the electron diffraction scattering derives primarily from the ordered phases, the relatively large fraction of the particle volume occupied by the disordered shells is probably responsible for a poor electron diffraction pattern. The core/shell structure was not observed for the two-phase particles. Figure 3b shows that many of these particles are not single crystals, but rather have multiple faults that also contribute to decreased diffraction intensity. The FFT of the particle shown by the arrow gives a d -spacing of 2.268 Å for (111) planes. The values of the d -spacing obtained from FFTs, for both the one- and two-phase Pd–C12 particles, are slightly larger than those of bulk palladium, in agreement with the electron diffraction data.

Behavior at the Air/Water Interface. Solutions of one-phase and two-phase Pd–C12 particles were prepared at a concentration of 1 mg/mL. Aliquots (200 μ L) were then spread at the air/water interface in a Langmuir–Blodgett trough. Visual observation indicated that the solution consisting of the one-phase Pd–C12 particles did not spread on the water surface and produced regions of large aggregates. After evaporation of the solvent, the particle film appeared hydrophobic and dewetted from the water surface. This phenomenon was not unexpected. In contrast to the results of M. Fukuto et al.,²² where the particles were functionalized with carboxylic groups, the thiol chains covering our particles are hydrophobic and the particles cannot be spread at the water interface.

A similar solution was also made from the two-phase Pd–C12 particles. In this case, the solution spread easily on the water

(19) Newville, M. J. *Synchrotron Radiat.* **2001**, *8*, 322.

(20) Shen, C. M.; Su, Y. K.; Yang, H. T.; Yang, T. Z.; Gao, H. J. *Chem. Phys. Lett.* **2003**, *373*, 39–45.

(21) JCPDS-International Centre for Diffraction Data.

(22) Fukuto, M.; Heilmann, R. K.; Pershan, P. S.; Badia, A.; Lennox, R. B. *J. Chem. Phys.* **2004**, *120*, 3446–3459.

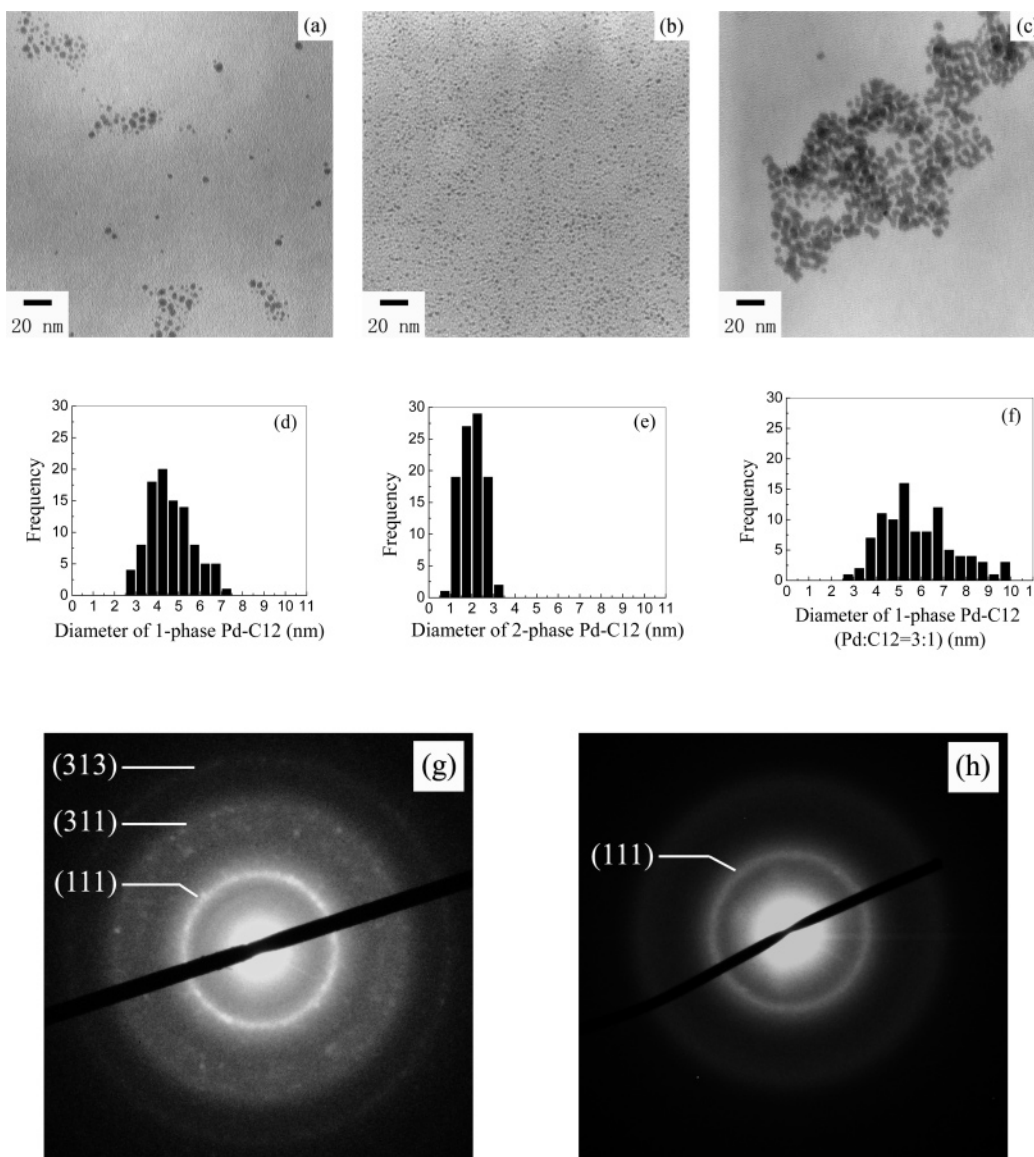


Figure 2. TEM pictures and core size distribution histograms of (a, d) one-phase Pd–C12 particles (Pd/C12 = 1:1), (b, e) two-phase Pd–C12 particles (1:1) and (c, f) one-phase Pd–C12 particles (3:1). Electron diffraction patterns of (g) one-phase Pd–C12 particles (1:1) and (h) two-phase Pd–C12 particles (1:1).

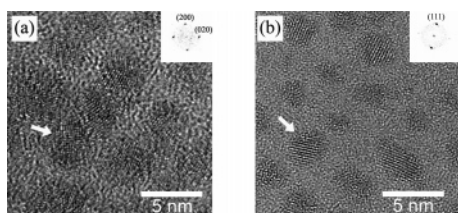


Figure 3. HRTEM pictures of (a) one-phase and (b) two-phase Pd–C12 particles inserted with FFT of the particles indicated by arrows.

surface. From auxiliary SIMS analysis of the films, we found traces of Br, which is a component of the amphiphilic surfactant used in the dissolution of the K_2PdCl_4 in toluene. This surfactant as residual impurity^{23,24} interdigitating with hydrophobic thiol chains may be responsible for the ability of these particles to wet the water surface.

The surface pressure vs area per particle (π – A) isotherm of this film is shown in Figure 4. From the figure, we find that there

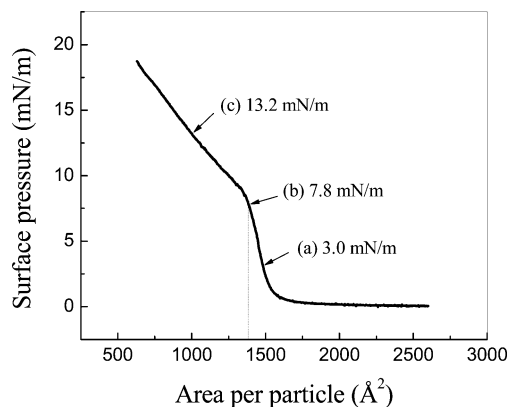


Figure 4. Isotherm π – A diagram of the two-phase Pd–C12 particles. At surface pressures of (a) 3.0, (b) 7.8, and (c) 13.2 mN/m, the films of particles were lifted onto solid substrates (TEM grids, silicon wafers, or Kapton films) for further examinations.

(23) Waters, C. A.; Mills, A. J.; Johnson, K. A.; Schiffrin, D. J. *Chem. Commun.* **2003**, *4*, 540–541.

(24) Leff, D. V.; Brandt, L.; Heath, J. R. *Langmuir* **1996**, *12*, 4723–4730.

is an abrupt onset pressure of 0.2 mN/m, followed by a shallow plateau region. To calculate how many particles had been spread, the average molecular weight of the particles was estimated as

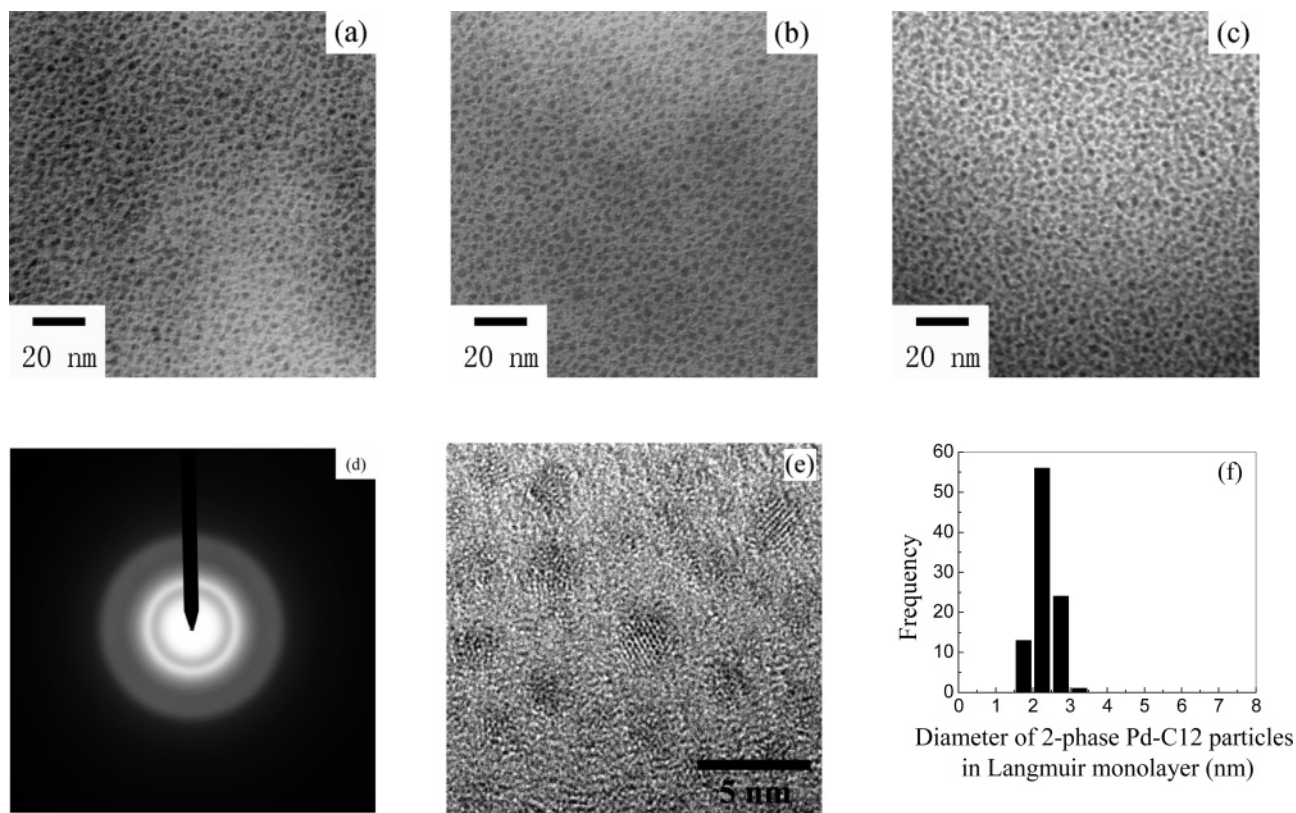


Figure 5. TEM pictures of two-phase Pd–C12 particles in thin films formed under (a) 3.0 mN/m, (b) 7.8 mN/m, (c) 13.2 mN/m, and (d) diffraction pattern, (e) HRTEM picture, and (f) size distribution histogram of particles in Langmuir monolayer (formed under 7.8 mN/m).

follows. Assuming an ideal cuboctahedral shape and fcc structure, there are 309 Pd atoms in one Pd core with a diameter of 20 Å. Assuming that each thiol chain occupies a surface area of 21.4 Å²,²⁵ there are about 60 thiol chains covering each core surface. Therefore, the average molecular weight is approximate 44 330 g/mol. From the phase diagram, we do not see a well-defined gas phase. As we will discuss later, the particles form an ordered film immediately after spreading. The film forms islands on the surface separated by bare areas of water. Hence, no pressure is built up until these islands become contiguous. Once that occurs, there is an immediate built up of pressure because the film is essentially solid. The plateau region is very shallow because the film is incompressible and easily collapses into a multilayered structure with increasing pressure.

Films were lifted from the water surface at pressures of 3.0, 7.8, and 13.2 mN/m onto TEM grids. The TEM and HRTEM images are shown in Figure 5. Here we can see that, at low pressures, the particles are still ordered locally, but large empty spaces are observed. As the pressure increases, a well-ordered array of nanoparticles is seen. While under the surface pressure of 13.2 mN/m, evenly dispersed single particles cannot be observed. These observations are consistent with the phase diagram. The kink in the isotherm was interpreted as the location where a solid monolayer is forming. At low pressures, we have a “gas” phase, while at higher pressures, the film collapses into a multilayer structure. At a surface pressure right below the kink (7.8 mN/m), the monolayer Langmuir film of two-phase Pd–C12 particles was deposited onto solid substrates, such as a TEM grid, silicon wafer, and Kapton film, and examined by electron microscopy, X-ray reflectivity, and EXAFS, respectively.

As given in Figure 5b, TEM micrograph of the monolayer Langmuir film shows a slightly larger particle size of 23 Å

compared with the size of two-phase Pd–C12 particles dried from dilute solution. The cell parameter a_0 , determined from electron diffraction, is about 3.94 Å, larger than 3.90 Å of bulk two-phase Pd–C12 particles. Therefore, we believe that the atomic positions in the two-phase Pd–C12 particles are changed after being spread at the air/water interface, although the particles still have fcc lattice structure.

The area/particle density in the monolayer Langmuir film is calculated to be 1310 Å² per particle according to the TEM image. This value agrees well with the density of 1385 Å² per particle at 7.8 mN/m based on the π - A isotherm.

X-ray Reflectivity. The Langmuir monolayer of two-phase Pd–C12 particles formed under surface pressure of 7.8 mN/m were deposited onto a silicon wafer and measured by X-ray reflectivity. A six-layer model was employed to simulate the structure of the film by nonlinear least-squares fitting. These six layers are Si substrate, SiO₂, thiol (hydrocarbon), Pd/thiol, thiol, and air, respectively. In Figure 6, the measured reflectivity as a function of the wave-vector transfer (q_z) and its best-fit based on the six-layer model (solid line), the model, and the dispersion (δ) value in the X-ray refractive index as a function of depth are illustrated. The fitting parameters are given in Table 1. The thickness of the top and bottom thiol layer is about 7.2 and 12.5 Å, respectively. Both of them are less than 15.6 Å, the length of a fully extended dodecanethiol chain,²⁶ which suggests the thiol chains are not perpendicular to the surface of the particle cores. We also find that there is no void in the top thiol layer because δ of this thiol layer is nearly the same as that of the bulk thiol. However, δ of the bottom thiol layer is 0.53 of the bulk thiol, indicating some thiol chains were removed from the Pd core surface. Therefore, the surface is more hydrophilic and allows the particles to spread at the air/water interface.

(25) Sellers, H.; Ulman, A.; Schmidman, Y.; Eilers, J. E. *J. Am. Chem. Soc.* **1993**, *115*, 9389–9401.

(26) Whetten, R. L.; Shafiqullin, M. N.; Khoury, J. T.; Schaaff, T. G.; Vezmar, I.; Alvarez, M. M.; Wilkinson, A. *Acc. Chem. Res.* **1999**, *32*, 397–406.

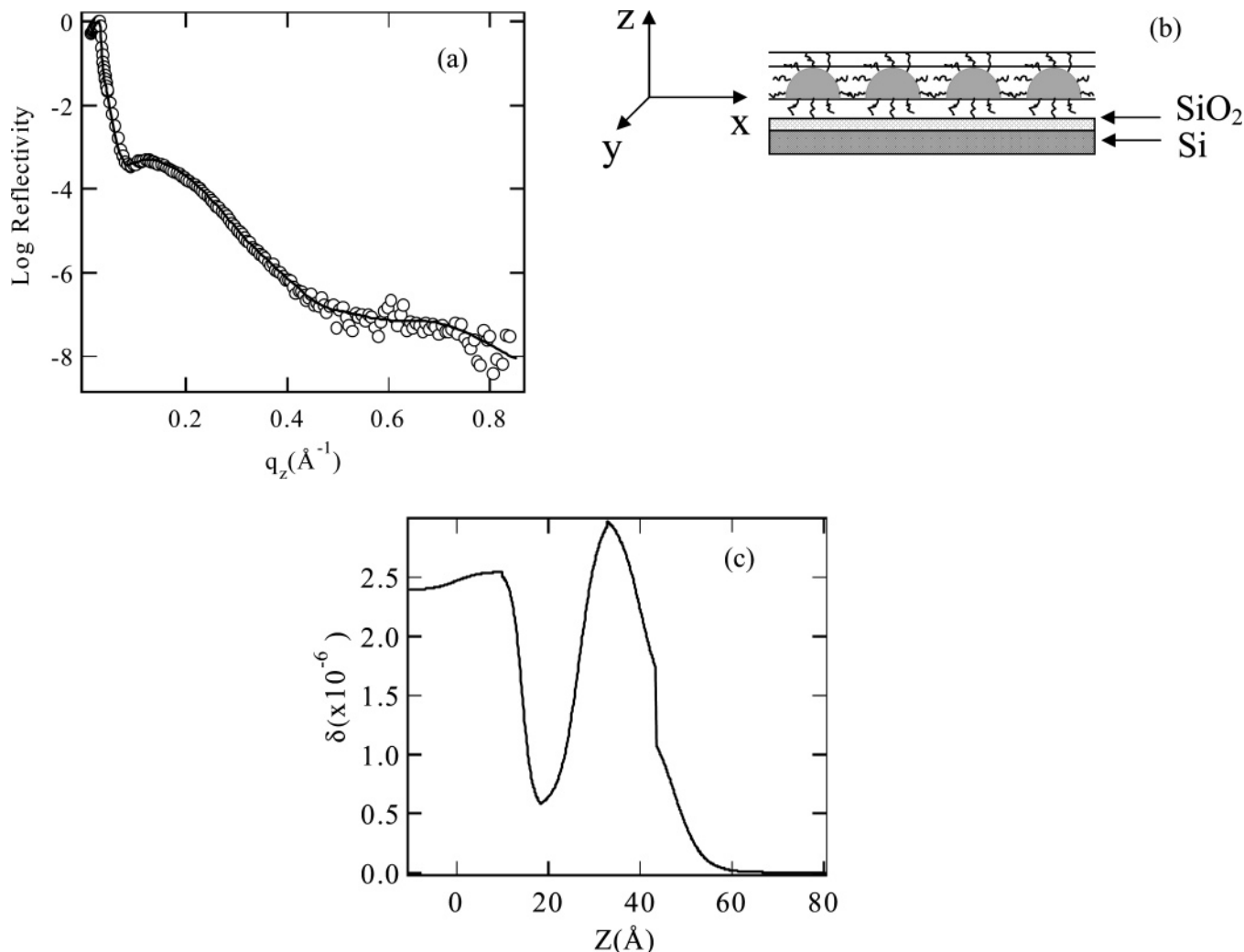


Figure 6. (a) Plot of the measured (empty circles) and the calculated (solid lines) reflectivities of the two-phase Pd–C12 Langmuir monolayer taken at surface pressure of 7.8 mN/m. (b) Scheme of the model of nanoparticle monolayer on a silicon wafer, (c) dispersion profile.

Table 1. X-ray Reflectivity Fitting Parameters for Two-Phase Pd–C12 Langmuir Monolayer, Where s Is the Roughness under Each Layer in Å, t Is the Average Thickness of a Layer in Å, and δ Is the Dispersion Component

	s	t	$\delta \times 10^6$
air	5.5		
thiol	4.5	7.2	1.0
Pd/thiol	5.0	13.3	3.1
thiol	3.0	12.5	0.53
SiO ₂		13.0	2.54
Si substrate			2.239

The thickness of the Pd/thiol layer is calculated to be about 13.3 Å, which can be considered as the diameter of the two-phase Pd–C12 particles in direction (Z) normal to the surface. The size measured from the TEM picture in Figure 5b is actually the average diameter of particles in X – Y plane (23 Å). If we assume the two-phase Pd–C12 particles are initially spherical when they are synthesized because there is no preferred symmetry in the synthesis, their diameter in every direction should be 20 Å. The decrease of average diameter in the Z -direction and increase in the X – Y plane suggest that the particles may change their shapes from spherical to oblate with an axial ratio of 0.57 after exposure to the water surface (Figure 7). To estimate the uncertainty of the thickness, we should take account of the interfacial roughness above and below this Pd/thiol layer, 4.5 and 5.0 Å, respectively. The uncertainty of the thickness is obtained from adding these values in quadrature to yield a value

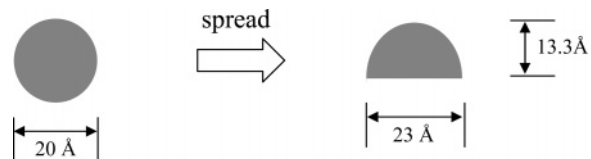


Figure 7. Two-phase Pd–C12 particles may change their shapes after being spread at the air/water interface.

of the thickness of the Pd/thiol layer as 13.3 ± 6.7 Å. The fairly large roughness can be seen to arise from the fact that the layer is composed of particles, rather than a uniform layer of deposited metal.

The scattering length density (SLD) of a mixed layer is the sum of the volume ratio of each component's SLD. For the mixed Pd/thiol layer,

$$SLD_{\text{Pd/thiol}} = SLD_{\text{Pd}}X_{\text{Pd}} + SLD_{\text{thiol}}X_{\text{thiol}} \quad (1)$$

$$X_{\text{Pd}} + X_{\text{thiol}} = 1 \quad (2)$$

where X_{Pd} and X_{thiol} are the volume fractions of Pd and thiol, respectively. SLD is related to δ by

$$SLD = \frac{2\pi}{\lambda^2} \delta \quad (3)$$

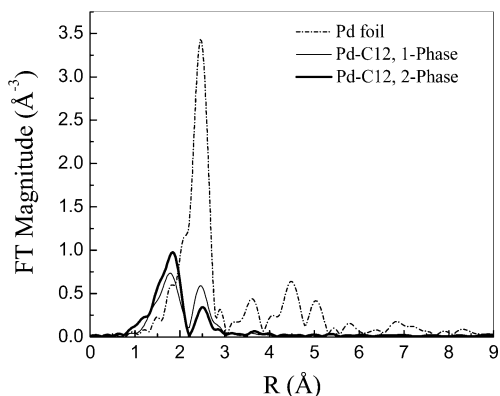


Figure 8. Fourier transformed EXAFS data of the reference palladium foil and the Pd–C12 nanoparticles.

where λ is the wavelength of the X-ray. Then,

$$\delta_{\text{Pd/thiol}} = \delta_{\text{Pd}}X_{\text{Pd}} + \delta_{\text{thiol}}X_{\text{thiol}} \quad (4)$$

$$\delta_{\text{Pd/thiol}} = 10.5 \times 10^{-6}X_{\text{Pd}} + 1.0 \times 10^{-6}X_{\text{thiol}} \quad (5)$$

For the Langmuir monolayer formed under surface pressure of 7.8 mN/m, when $\delta_{\text{Pd/thiol}}$ is best fit to be 3.1×10^{-6} as shown in Table 1, X_{Pd} is calculated to be 0.221. So the Pd cores occupy approximately a quarter volume of the mixed Pd/thiol layer. Assuming the Pd cores obtain an oblate geometry as in Figure 6, the area/particle density in the monolayer can be estimated to be 1384 \AA^2 , which is consistent with the values calculated from the TEM image (1310 \AA^2) and the π -A isotherm (1385 \AA^2).

EXAFS Analysis. EXAFS can be used to estimate the mean crystallite size of nanocrystalline material due to the termination effect that describes the phenomenon of lowered average coordination numbers arising from surface atoms having fewer neighbors. The average coordination number of nearest neighbors (CN) in nanoparticles is a nonlinear function of the particle size.^{27–31} The Fourier transforms (FTs) of all EXAFS data are presented in Figure 8, where the characteristic signatures of the fcc structure in the reference Pd foil data can be found in the FT spectra of both one- and two-phase Pd–C12 particles. Besides, there is an additional peak below 2 \AA (uncorrected for the photoelectron phase shifts) in the FT spectra of the particles compared with that of the Pd foil. This peak corresponds to the first nearest neighbors Pd–S bond. Theoretical scattering amplitudes and phases of the photoelectron are calculated with program FEFF6.³² FT spectra and best fits considering the contributions from both Pd–Pd and Pd–S bonds are shown in Figure 9. During the fitting procedures, the data and the theory were k -weighted and Fourier transformed by using a Hanning window function in the k -range from 2 to 10 \AA^{-1} . The fitting ranges were from 1.2 to 3 \AA . Results of the fitting are summarized in Table 2. The coordination numbers CN(Pd–Pd) of the one- and two-phase Pd–C12 particles are 4.0 ± 0.9 and 2.3 ± 1.0 , respectively. Assuming cuboctahedral structural motif of Pd nanoparticles, and the homogeneity of the sample (i.e., all Pd atoms are in the crystalline nanoparticle phase), these coordination numbers correspond to the particle sizes of smaller than 10 \AA

for both one- and two-phase Pd–C12 particles, which are much smaller than those determined from TEM measurements. Therefore, we need to reexamine the interpretation of the EXAFS results. The assumption that all Pd particles are in the crystalline nanoparticle phase may not be true if the particles had begun to decompose, as suggested by Chen et al.,³³ or some palladium–thiol and/or palladium–sulfide complexes had been formed outside the particles.^{15,16,18} For the one-phase Pd–C12 particles, HRTEM analysis had revealed an ordered core with a disordered shell structure. In this case, only a fraction, x , would be coordinated in the Pd particle cores, while the rest would be in a disordered state surrounding the cores. This fraction can be determined from the equation

$$x = \frac{N_{\text{C}}}{N_{\text{P}}} \quad (6)$$

where N_{C} is the number of molecules of palladium–sulfide compounds (a cumulative name for different types of low-molecular-weight Pd–S complexes that may be present in the sample and that we are not attempting to identify), and N_{P} the number of Pd–C12 nanoparticles.

EXAFS analysis results in the average coordination number, ν , of the Pd–Pd first nearest neighbors,

$$\nu = \frac{2N_{\text{B}}}{N_{\text{A}}} \quad (7)$$

where N_{A} is the total number of Pd atoms, and N_{B} is the total number of first nearest neighbor Pd–Pd bonds in the sample. In this approximation of the ordered core/disordered shell, only the Pd atoms in the ordered cores of the particles have nearest neighbor Pd–Pd bonds. Therefore, the best fit result for ν would agree with the average coordination number of the Pd–Pd first nearest neighbors only if the sample is homogeneous, e.g., it contains the single phase of dodecanethiolate palladium particles. However, the Pd atoms in the disordered region also contribute to the X-ray absorption signal. This has the effect of reducing the observed Pd–Pd coordination number compared to that in the single-phase system because the total number of Pd atoms, N_{A} , is now

$$N_{\text{A}} = N_{\text{P}} \times n_{\text{A}} + N_{\text{C}} \quad (8)$$

where n_{A} is the number of Pd atoms in a core. N_{B} (eq 7) can be determined as follows:

$$N_{\text{B}} = N_{\text{P}} \times n_{\text{B}} \quad (9)$$

where n_{B} is the number of Pd–Pd bonds in a core.

Therefore, the ratio of N_{C} versus N_{P} , x , could be obtained from eq 10 if the number of Pd atoms in a core (n_{A}) and the number of Pd–Pd bonds in a core (n_{B}) are known experimentally or theoretically.

$$x = \frac{2n_{\text{B}}}{\nu} - n_{\text{A}} \quad (10)$$

HRTEM measurements yielded the mean core size of $26 \pm 8 \text{ \AA}$. Assuming a cuboctahedral structure with fcc symmetry, n_{A} and n_{B} in an ordered core can be determined. Although the two-phase Pd–C12 particles do not have the core/shell structure, they are heterogeneous; both the Pd nanoparticles and the Pd–S compounds are present in the samples, as communicated by too-

(27) Clausen, B. S.; Topsøe, H.; Hansen, L. B.; Stoltze, P.; Nørskov, J. K. *Catal. Today* **1994**, *21*, 49–55.

(28) Benfield, R. E. *J. Chem. Soc., Faraday Trans.* **1992**, *88*, 1107–1110.

(29) Greigor, R. B.; Lytle, F. W. *J. Catal.* **1980**, *63*, 476–486.

(30) Jentys, A. *Phys. Chem. Chem. Phys.* **1999**, *1*, 4059–4063.

(31) Frenkel, A. I. *J. Synchrotron Radiat.* **1999**, *6*, 293–295; Frenkel, A. I.; Hills, C. W.; Nuzzo, R. G. *J. Phys. Chem. B* **2001**, *105*, 12689–12703.

(32) Zabinsky, S. I.; Rehr, J. J.; Ankudinov, A.; Albers, R. C.; Eller, M. J. *Phys. Rev. B* **1995**, *52*, 2995–3009.

(33) Chen, S.; Huang, K.; Stearns, J. A. *Chem. Mater.* **2000**, *12*, 540–547.

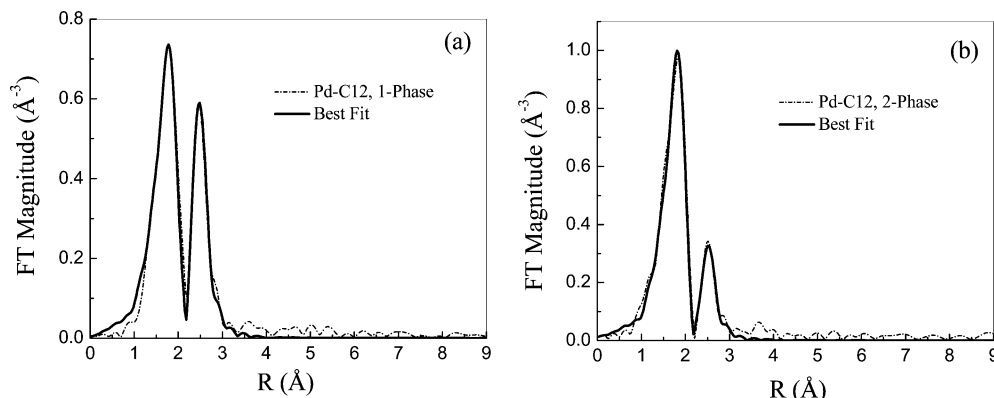


Figure 9. Data and FEFF6 fit of (a) one-phase and (b) two-phase Pd–C12 particles.

Table 2. Summary of Results of EXAFS Refinements of Palladium Foil and the Pd–C12 Particles^a

	CN(Pd–Pd)	R(Pd–Pd) (Å)	σ^2 (Pd–Pd) (Å ²)	CN(Pd–S)	R(Pd–S) (Å)	σ^2 (Pd–S) (Å ²)
palladium foil	12	2.726(2)	0.0050(3)			
one-phase Pd–C12	4.0(9)	2.74(1)	0.0096(15)	2.2(4)	2.29(1)	0.0056(18)
two-phase Pd–C12	2.3(1.0)	2.77(2)	0.0102(40)	2.9(5)	2.31(1)	0.0044(14)

^a CN, R, and σ^2 are the coordination number, interatomic distance, and the standard deviation in the distance between the central (absorbing) Pd atom and its nearest (S or Pd) neighbors. Uncertainties in the last digits are given in parentheses.

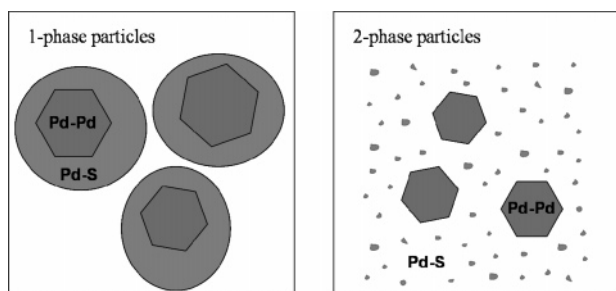


Figure 10. Models of one- and two-phase Pd–C12 particles illustrate the association of the disordered Pd–S compounds with the particles.

Table 3. Summary of Component Analysis of Pd–C12 Particles

	core size (Å) (HRTEM)	n_A	n_B	ν	x
one-phase Pd–C12	26	561	2820	4.0	849
two-phase Pd–C12	20	309	1488	2.3	985

small Pd–Pd and too-large Pd–S (compared to a homogeneous model) coordination numbers obtained from EXAFS. Therefore, eqs 7–10 can be applied to this case as well. The only difference is that the “ordered cores” are the Pd particles themselves. The results of the reexamination of EXAFS data are summarized in Table 3, which demonstrates that a large amount of Pd–S compounds are associated with one-phase and two-phase Pd–C12 particles. On the basis of HRTEM and EXAFS studies, the nature of the Pd–C12 particles can be illustrated in two models in Figure 10: for the one-phase Pd–C12 particles, Pd–S compounds form disordered shells covering ordered Pd cores, while for the two-phase Pd–C12 particles, Pd–S compounds loosely exist around the particles.

As shown in Table 2, the length of the Pd–Pd bonds, 2.74 and 2.77 Å for the one-phase and two-phase Pd–C12 particles, respectively, are slightly longer than that of the bulk palladium. This phenomenon of lattice expansion has also been suggested by HRTEM and electron diffraction data mentioned above. It is known that the lattice contraction is common in metal nanoparticles^{34–36} due to their large surface tension.^{35a,37} On the

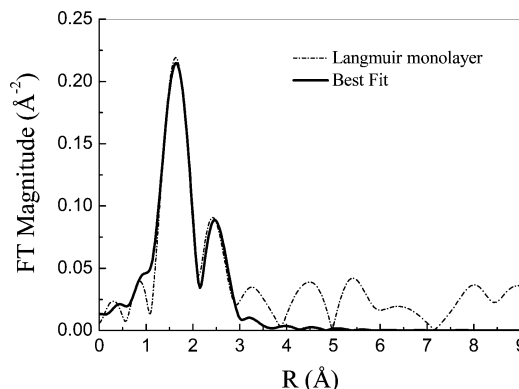


Figure 11. Data and FEFF6 fit of Langmuir monolayer of two-phase Pd–C12 particles.

contrary, the lattice expansion has been observed by other researchers^{38–41} in Pd nanoparticles, attributed to a structural change,³⁸ pseudomorphism,⁴⁰ or unresolved reason.⁴¹ In our case, because the outer surface of the one-phase particles consists of the disordered shell, the expansion may occur to accommodate the enhanced surface disorder.

A stack of 750 Langmuir monolayers of the two-phase Pd–C12 particles was used to obtain EXAFS data. The FT spectrum and its best fit are given in Figure 11. The fitting results are compared in Table 4 with those of the two-phase Pd–C12 particles before being exposed to the water surface. The coordination number CN(Pd–Pd) of the two-phase Pd–C12 particles in the Langmuir monolayer is 6.0 ± 2.0 , larger than that of two-phase Pd–C12 particles in bulk. Because we believe that the existence

(34) Berry, C. R. *Phys. Rev.* **1952**, *88*, 596–599.

(35) (a) Vermaak, J. S.; Mays, C. W.; Kuhlmann-Wilsdorf, D. *Surf. Sci.* **1968**, *12*, 128. (b) Mays, C. W.; Vermaak, J. S.; Kuhlmann-Wilsdorf, D. *Surf. Sci.* **1968**, *12*, 134. (c) Wassermann, H. J.; Vermaak, J. S. *Surf. Sci.* **1972**, *32*, 168.

(36) Montano, P. A.; Zhao, J.; Ramanathan, M.; Shenoy, G. K.; Schulze, W.; Urban, J. *Chem. Phys. Lett.* **1989**, *164*, 126–130.

(37) Woltersdorf, J.; Nepijko, A. S.; Pippel, E. *Surf. Sci.* **1981**, *106*, 64–69.

(38) Heinemann, K.; Poppa, H. *Surf. Sci.* **1985**, *156*, 265–274.

(39) Giorgio, S.; Henry, C. R.; Chapon, C.; Penisson, J. M. *J. Cryst. Growth* **1990**, *100*, 254–260.

(40) Goyhenex, C.; Henry, C. R.; Urban, J. *Philos. Mag. A* **1994**, *69*, 1073–1084.

(41) Teranishi, T.; Miyake, M. *Chem. Mater.* **1998**, *10*, 594–600.

Table 4. Comparison of Results of EXAFS Refinements of the Two-Phase Pd–C12 Particles before and after Exposure to Water Surface

	CN(Pd–Pd)	R(Pd–Pd) (Å)	σ^2 (Pd–Pd) (Å ²)	CN(Pd–S)	R(Pd–S) (Å)	σ^2 (Pd–S) (Å ²)
two-phase Pd–C12	2.3(1.0)	2.77(2)	0.0102(40)	2.9(5)	2.31(1)	0.0044(14)
monolayer films	6.0(2.0)	2.76(2)	0.0175(72)	2.5(6)	2.25(1)	0.0000(35)

of palladium–sulfide compounds is the reason for the reduced coordination number CN(Pd–Pd) of the bulk two-phase Pd–C12 particles, there is a possibility that a portion of the compounds is removed from the two-phase Pd–C12 particles when they are being spread onto the air/water interface. This result was consistent with the HRTEM images, which indicated that the Pd–S compounds were not strongly attached to the particle surface and hence may have dissolved in the water. The rest of the compounds covering the particles again play a role in decreasing the apparent coordination number CN(Pd–Pd) of the Langmuir monolayer. As we mentioned in the previous part, the particles in the monolayer might have an oblate shape. On the basis of the coordination number, we can assume an fcc packing model of three layers, consisting of 82 Pd atoms, as illustrated in Figure 12. This model gives a particle diameter of 19.3 Å, which is somewhat smaller than that observed by using TEM. The discrepancy in the diameter may be due to the fact that TEM measures the entire particle, where both particle and Pd–S compounds are present. On the other hand the EXAFS result is determined by the portion of the film that has a well-defined Pd–Pd nearest neighbor coordination number. The model in Figure 12 also gives a Pd/thiol layer thickness of 6.7 Å, which again is smaller than the X-ray reflectivity calculated thickness of 13.3 Å. In this case, the agreement may be even better if we consider that the X-ray reflectivity value reflects the average thickness, including both the particles and the Pd–S compounds, as illustrated in Figure 13.

Langmuir Films of Two-Phase Pd–C18 Particles. Although covered by longer thiol chains, the two-phase Pd–C18 particles have similar behavior to the two-phase Pd–C12 particles at the air/water interface. They can also be spread and form a Langmuir monolayer upon compression. To understand the Langmuir films of two-phase Pd–C18 particles and compare them with those of two-phase Pd–C12 particles, specular reflectivity was used to determine the film thickness as a function of the surface pressure, while GIXD was used to determine the in-plane order of the particles. According to the π - A isotherm given in Figure 14, the Langmuir films of two-phase Pd–C18 were vertically lifted onto silicon wafers at surface pressures of 0.2, 15, and 55 mN/m, respectively.

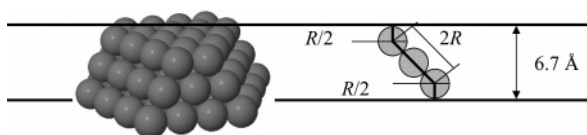


Figure 12. Truncated cuboctahedron model with three layers of Pd atoms and a coordination number of 7.98, giving a particle diameter of 19.3 Å and Pd/thiol thickness of 6.7 Å. R is the interatomic distance of Pd atoms.

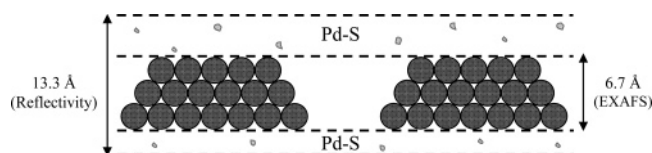


Figure 13. Illustration of Pd/thiol layer thickness, using thickness from EXAFS and X-ray reflectivity.

In Figure 15, the measured reflectivities as function of q_z (wave-vector transfer) for the Langmuir films formed under these three surface pressures are plotted. At low pressure (0.2 mN/m), the amplitude of the Kiessig fringes is not clear, indicative of a nonuniform layer with a large surface roughness. When the surface pressure reaches 15 mN/m, there is a slight increase in the frequency of the Kiessig fringes, and the amplitude becomes much more pronounced, implying that the film becomes laterally uniform. The sample prepared under 55 mN/m results in a higher frequency of the Kiessig fringes corresponding to a thicker film. Besides, the interference fringes persist to large q_z , and the oscillations become more pronounced, indicating that the structures of more than one layer are laterally uniform to the substrate surface.

The best fits to the reflectivities of the Pd–C18 films are shown as solid lines in Figure 15a, and the corresponding density profiles are displayed in Figure 15b. We can see that a monolayer of palladium particles is formed under a surface pressure of 15 mN/m. The fit gives the thickness of the Pd/thiol layer of 13 Å, while the average diameter of the Pd cores is determined to be 39 Å based on the TEM image of the monolayer film. Therefore, the two-phase Pd–C18 particles on the water surface are actually platelets, in agreement with the previous observations on the two-phase Pd–C12 particles.

Further compression to 55 mN/m produces a second Pd/thiol layer with a low-density region between the two Pd/thiol layers, as shown by dashed lines in Figure 15b. This low-density dip corresponds to a layer between the two Pd/thiol layers filled by the alkyl chains. To obtain in-plane information, we measured GIXD of the two-phase Pd–C18 Langmuir films. Figure 16 shows the GIXD amplitude for two-phase Pd–C18 on Si substrate plotted against q_{xy} . It should be noted that the same samples for XR were used for GIXD measurements. At low surface pressure, no peak is observed, indicating that no ordered structure is present at this pressure. This is in agreement with the nonuniform layer shown by XR. The measurements for samples made at 15 and 55 mN/m show similar peaks at $q_{xy} = 0.167 \text{ \AA}^{-1}$ (fitted by a Lorentzian function), but no higher-order peaks are observed. If one assumes that the nanoparticles form a hexagonal close-packed structure, the position q_{xy} corresponds to an interparticle spacing

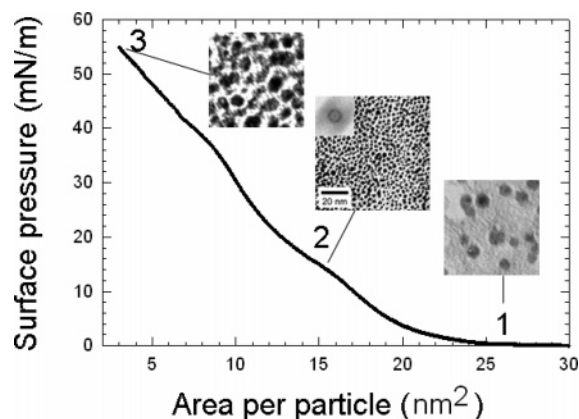


Figure 14. Isotherm π - A diagram of the two-phase Pd–C18 particles. Inserts are TEM images of the Langmuir films formed under certain surface pressures.

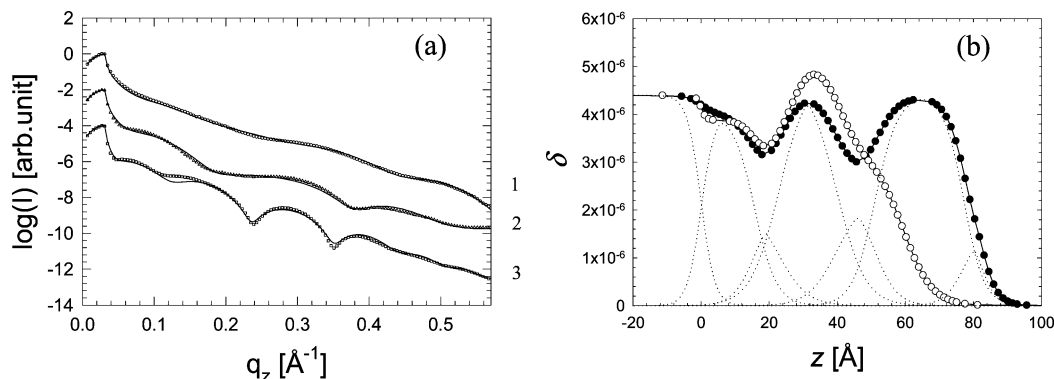


Figure 15. (a) Specular X-ray reflectivities (symbols) and fits (solid lines) of two-phase Pd–C18 Langmuir films lifted onto silicon wafers at (1) $\pi = 0.2$, (2) 15, and (3) 55 mN/m. The reflectivity curves are shifted for clarity. (b) Density profiles at 15 mN/m (open circles) and 55 mN/m (solid circles). The dotted lines are the components that form the electron density model of $\pi = 55$ mN/m.

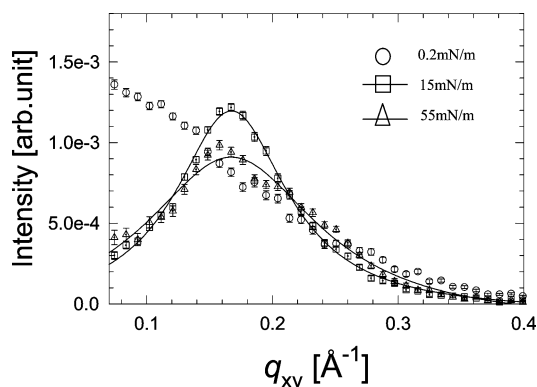


Figure 16. GIXD amplitude for two-phase Pd–C18 Langmuir films plotted against q_{xy} .

of $a = 4\pi/\sqrt{3}q_{xy} = 43.3 \text{ \AA}$. We can also see that the peak position is fairly insensitive to the surface pressures, but only a slight decrease in the peak intensity is observed. This indicates that the interparticle spacing remains fairly constant with pressure and does not change while the film undergoes a spectrum of transitions ranging from monolayer coverage to collapse. The peaks are broadened, which indicates that there is no long-range order in the monolayer. The inset of Figure 14 shows a TEM image of the Langmuir monolayer as well as the Fourier transform of the image. The radius of the ring corresponds to the interparticle distance of about 40 \AA , which is in good agreement with the GIXD result.

Conclusions

In this work, we compare the characteristics of Pd–C12 nanoparticles synthesized by two different techniques, a one-phase method and a two-phase method. Transmission electron microscopy determines that the mean particle sizes are 46 and 20 \AA for the one- and two-phase Pd–C12 particles, respectively. Electron diffraction confirms that their structure is fcc, with a lattice constant a_0 of 3.98 and 3.90 \AA for the one- and two-phase particles, respectively. High-resolution TEM reveals an ordered

core/disordered shell structure for the one-phase particles and a crystalline nature for the two-phase particles. Examination of the EXAFS data reveals particle sizes much smaller than those measured by TEM if a cuboctahedral fcc structural model of Pd particles surrounded by thiol is assumed. Therefore, we propose a model that contains a large amount of disordered palladium–sulfide compounds along with the metallic particle cores. According to HRTEM results, these disordered Pd–S compounds form shells embedding ordered cores for the one-phase particles, while they loosely exist with crystalline two-phase particles. Compared with the bulk palladium, lattice expansion is observed in both one- and two-phase particles by electron diffraction, HRTEM, and EXAFS.

A Langmuir monolayer of the two-phase Pd–C12 particles can be manufactured by using the Langmuir–Blodgett technique. X-ray reflectivity shows that the thickness of this layer is only $13 \pm 7 \text{ \AA}$, while TEM shows that the diameter of the particles in this layer is $23 \pm 3 \text{ \AA}$. Hence, the particles in the monolayer are oblate. This structure is also consistent with the EXAFS data, which could be fit if a truncated cuboctahedron model with three layers of Pd atoms is assumed. The large aspect ratio of this film gives it unique electronic properties and increases the surface-to-volume ratio, which may enhance its catalytic capacity.

Acknowledgment. We acknowledge support by the NSF-MRSEC program and the U.S. Department of Energy grant no. DE-FG02-03ER15477 (A.I.F.). NLSL is supported by the Divisions of Materials and Chemical Sciences of DOE. Research carried out in part at the Center for Functional Nanomaterials, Brookhaven National Laboratory, which is supported by the U.S. Department of Energy, Division of Materials Sciences, and Division of Chemical Sciences, under contract no. DE-AC02-98CH10886. The authors gratefully acknowledge Dr. James Quinn for assistance with TEM measurements, Hongwen Zhou for assistance with electron diffraction indexing, Dr. Lijun Wu for assistance with HRTEM image analysis, and Avital Merl and Dana Glasner for assistance with the EXAFS data collection and analysis.

LA052686K